A Four-Dimensional Plus Hysteresis Chaos Generator

Kunihiko Mitsubori and Toshimichi Saito, *Member, IEEE*

***Abstract*— This paper discusses a four-dimensional plus hysteresis autonomous chaotic circuit. The circuit dynamics is described by two symmetric four-dimensional linear equations connected to each other by hysteresis switchings. We transform the equation into Jordan form and derive theoretical formulas of its three-dimensional return map, its Jacobian matrix and its Jacobian. These formulas can be developed easily to general dimensional cases and are used to evaluate Lyapunov exponents. Then we have discovered torus doubling route to chaos and then to hyperchaos. Some of the return map attractors are confirmed by laboratory experiments. A rough two parameters bifurcation diagram is also given.**

I. Introduction

CHAOTIC phenomena in electric circuits have been studied with great interest. In the study of autonomous chaotic circuits, some interesting results are given for three-dimensional (3-D) systems [1]–[5], and some experimental results are given for four-dimensional (4-D) ones [6]–[8]. Then more higher dimensional systems have been recently begun to investigate [9].

More than 3-D circuits can exhibit hyperchaos [6] and related interesting phenomena which cannot be observed in 3-D ones. Hyperchaos is a higher dimensional chaos introduced by Rössler [7] and is usually defined as a chaotic attractor with more than one positive Lyapunov exponent. It implies that its dynamics expand more than one direction. They relate important fundamental problems: classification of chaos, route to chaos and so on [10], [11]. Also analysis and synthesis of such circuits may contribute to engineering applications, among them: spread spectrum communications [12], [13], controlling chaos [14]–[16] and memory search in artificial neural networks [17]. However, the analysis of more than 3-D chaotic circuits is difficult because of the system complexity. In order to approach to such a circuit, we should focus on a simple model.

Then, this paper considers a 4-D plus hysteresis autonomous circuit given by Fig. 1(a). Here, $-r_1$ and $-r_2$ are linear negative resistors characterized by $v'_j = -r_j i_j$ $(j = 1, 2)$. In experiments, we utilize the central part of a current-controlled nonlinear resistor characterized by Fig. 1(b). Fig. 1(c) gives its implementation example. $-H$ is a dependent voltage source characterized by the following hysteresis (see Fig. 1(d)):

$$-H(v_1 + v_2) = \begin{cases} E & \text{for } v_1 + v_2 \geq -Er_a/r_b \\ -E & \text{for } v_1 + v_2 \leq Er_a/r_b \end{cases}. \quad (1)$$

$-H$ is switched from E to $-E$ if $v_1 + v_2$ hits the left threshold $-Er_a/r_b$ and vice versa. Fig. 1(e) gives an implementation example of $-H$. Here, $-H$ consists of inverting adder and hysteresis comparator. Hereafter, we assume that the op amp is linear and that the zener diode is ideal. The circuit dynamics can be described by two symmetric linear equations connected to each other by a hysteresis switchings:

$$\begin{aligned} \mathrm{RC}\frac{dv_1}{dt} &= Ri_1 - (v_1 + H(v_1 + v_2)), L_1\frac{di_1}{dt} = -v_1 + r_1 i_1 \\ \mathrm{RC}\frac{dv_2}{dt} &= Ri_2 - (v_1 + H(v_1 + v_2)), L_2\frac{di_2}{dt} = -v_2 + r_2 i_2. \end{aligned} \quad (2)$$

Here the vector field of the state variables consists of two overlapping 4-D halfspaces.

Such hysteresis chaos generators have been developed by Newcomb's group and us. Newcomb and El-leithy have proposed a chaos generator that includes binary hysteresis [2] in 1984. Contemporarily, the second author has proposed a hysteresis chaos generator based on a quasi-harmonic oscillator [18]. Also we show a chaotic circuit family that includes one hysteresis resistor in [19] and the normal form equation from five-dimensional case is equivalent to (7) in some parameter range. The hysteresis resistor can be realized by three segments piecewise linear resistor for which a small inductor L_0 is connected in series. Letting L_0 tend to zero, the piecewise linear resistor is to be hysteresis one. Then the 3- and 4-D circuit can be treated as 2- and 3-D plus hysteresis one, respectively. In these cases, we have given a sufficient condition for chaos generation under strong parameter restriction [5], [8]. Chua's circuit includes a three segments piecewise linear resistor and some interesting results are given by using piecewise linear techniques [20], [21]. The 2-D plus hysteresis chaos generator [2], [5] is a limiting case of Chua's circuit and its analysis procedure is simpler because of hysteresis switching of two linear systems.

This circuit exhibits interesting phenomena. Fig. 2 shows some examples of them as r_b/r_a decreases. Fig. 2(a) shows a periodic orbit. This circuit has two different resonance frequencies controlled by two inductors L_1 and L_2, respectively, and their interaction affects the dynamics. As r_b/r_a decreases, the attractor changes to torus Fig. 2(b) and then to chaotic attractors Fig. 2(c) and (d). The chaos Fig. 2(d) has different

Manuscript received April 11, 1994; revised September 5, 1994. This paper was recommended by Associate Editor Michael Peter Kennedy.

The authors are with the Department of Electrical and Electronical Engineering, HOSEI University, Koganei-shi, Tokyo, 184 Japan.

IEEE Log Number 9407179.

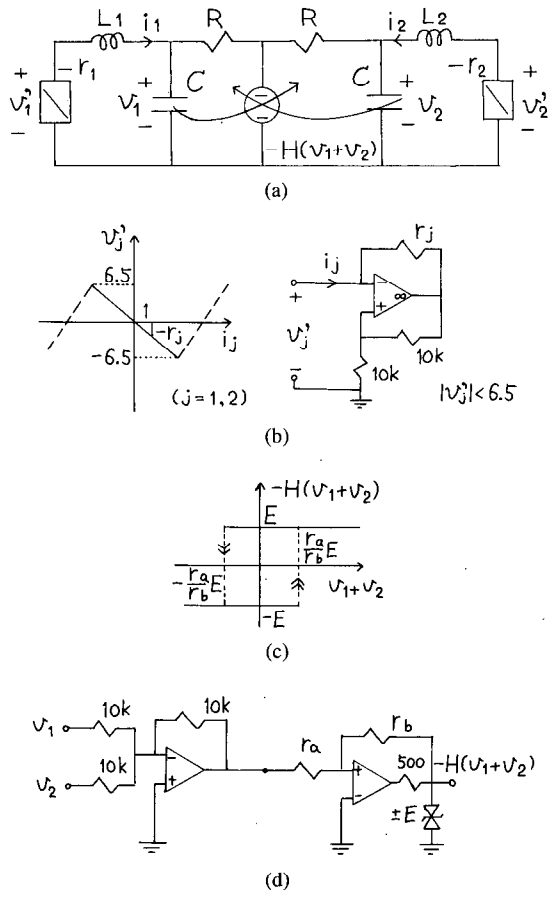

Fig. 1. A 4-D plus hysteresis chaos generator.

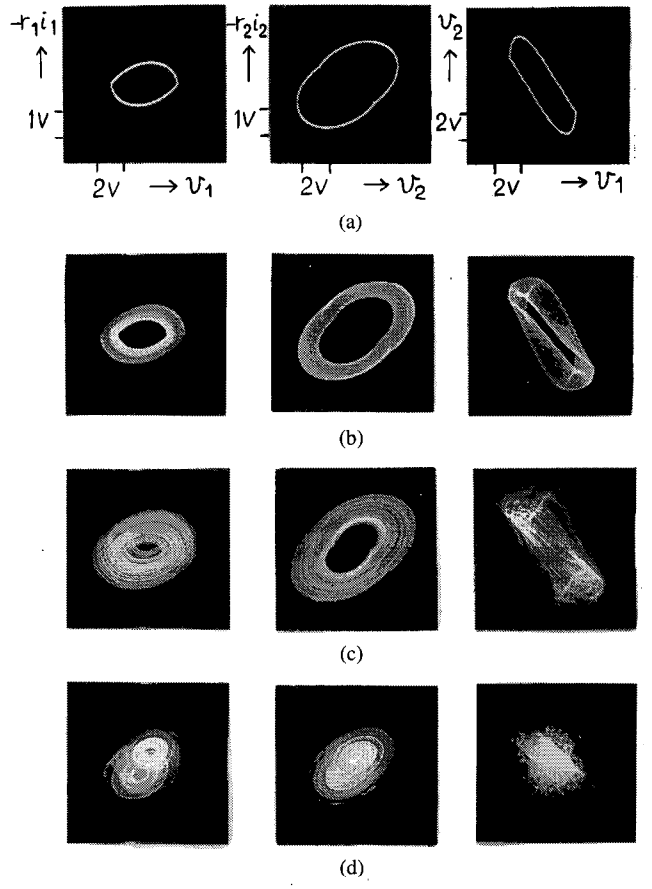

Fig. 2. Change of attractor as $\frac{r_b}{r_a}$ decreases ($C \simeq 10$ nF, $R \simeq 15$ kΩ, $L_1 \simeq 300$ mH, $L_2 \simeq 150$ mH, $r_1 \simeq 2.5$ kΩ, $r_2 \simeq 1.5$ kΩ). (a) Periodicity for $\frac{r_b}{r_a} = 3.8$; (b) torus for $\frac{r_b}{r_a} = 3.0$; (c) area expanding chaos ($\mu_2 > 0$) for $\frac{r_b}{r_a} = 2.0$; (d) volume expanding chaos ($\mu_3 > 0$) for $\frac{r_b}{r_a} = 1.3$.

topology from Fig. 2(c). This paper analyzes such phenomena by using a piecewise linear techniques. The outline is as the following:

1) We transform the circuit equation into Jordan form [22] and derive theoretical formulas of the 3-D return map, its Jacobian matrix and its Jacobian. These can be developed easily to general dimensional cases.
2) Using these formulas, we evaluate Lyapunov exponents [23], [24] for attractor from the return map. These exponents are used to classify the phenomena.
3) We select r_b/r_a as a control parameter. It controls the locations of the equilibrium points. Then we have discovered torus doubling route [25], [26] to area expanding chaos [27] that has positive 2-D Lyapunov exponent. We have also discovered volume expanding chaos that has positive 3-D Lyapunov exponent. The volume expanding chaos is a kind of hyperchaos. Some of the return map attractors are verified by laboratory measurements.
4) We calculate a rough two parameters bifurcation diagram in which L_2 is another control parameter. It suggests that the torus doubling route is not singular.

In this system, the analysis procedure can be developed easily for general dimensional plus hysteresis chaos generator. It can contribute to systematic analysis for the general dimensional case. This is the first circuit in which torus doubling route to area expanding chaos and volume expanding chaos are confirmed by both numerical experiments using piecewise linear exact solutions and laboratory experiments.

II. Jordan Form for the Hysteresis Circuit

Using dimensionless variables and parameters:

$$\tau' = \frac{t}{RC}, \quad \text{“}\cdot\text{”} = \frac{d}{d\tau'}, \quad \eta = \frac{r_b}{r_a}$$
$$X_1 = \frac{\eta v_1}{E}, \quad Y_1 = \frac{\eta R i_1}{E}, \quad X_2 = \frac{\eta v_2}{E}, \quad Y_2 = \frac{\eta R i_2}{E}, \tag{3}$$
$$\alpha_1 = \frac{R^2 C}{L_1}, \quad \beta_1 = \frac{r_1}{R}, \quad \alpha_2 = \frac{R^2 C}{L_2}, \quad \beta_2 = \frac{r_2}{R}.$$

Equation (2) is transformed into the following equation:

$$\begin{bmatrix} \dot{X}_1 \\ \dot{Y}_1 \end{bmatrix} = \begin{bmatrix} -1 & 1 \\ -\alpha_1 & \alpha_1\beta_1 \end{bmatrix} \left[\begin{bmatrix} X_1 \\ Y_1 \end{bmatrix} - \eta \begin{bmatrix} p_1 \\ p_1/\beta_1 \end{bmatrix} h(X_1 + X_2) \right],$$
$$\begin{bmatrix} \dot{X}_2 \\ \dot{Y}_2 \end{bmatrix} = \begin{bmatrix} -1 & 1 \\ -\alpha_2 & \alpha_2\beta_2 \end{bmatrix} \left[\begin{bmatrix} X_2 \\ Y_2 \end{bmatrix} - \eta \begin{bmatrix} p_2 \\ p_2/\beta_2 \end{bmatrix} h(X_1 + X_2) \right], \tag{4}$$

where

$$h(X_1+X_2) \equiv -H\left(\frac{E}{\eta}(X_1+X_2)\right)\Big/E = \begin{cases} 1 & \text{for } X_1+X_2 \geq -1 \\ -1 & \text{for } X_1+X_2 \leq 1 \end{cases},$$

$$p_1 \equiv \frac{\beta_1}{1-\beta_1}, \quad p_2 \equiv \frac{\beta_2}{1-\beta_2}.$$

The variable X_1, X_2, Y_1 and Y_2 are proportional to v_1, v_2, Ri_1 and Ri_2, respectively. h is a normalized hysteresis and is switched from 1 to -1 if X_1+X_2 hits the left threshold -1 and vice versa. This system has five parameters $(\alpha_1, \beta_1, \alpha_2, \beta_2, \eta)$. The parameter α_1 and α_2 control oscillation frequencies, β_1 and β_2 control dumping, and η controls the width of hysteresis thresholds. We focus on the case where the coefficient matrix of (4) has four complex eigenvalues $\Delta_1 \pm j\Omega_1$ and $\Delta_2 \pm j\Omega_2$:

$$\Delta_1 = \frac{\alpha_1\beta_1 - 1}{2}, \quad \Omega_1^2 = \alpha_1\beta - 1) - \frac{(\alpha_1\beta_1-1)^2}{4} > 0,$$
$$\Delta_2 = \frac{\alpha_2\beta_2 - 1}{2}, \quad \Omega_2^2 = \alpha_2(1-\beta_2) - \frac{(\alpha_2\beta_2-1)^2}{4} > 0. \tag{5}$$

Note that $(1-\beta_1)$ and $(1-\beta_2)$ must be positive hence p_1 and p_2 are positive. Then applying the transformation:

$$x_1 = X_1, \quad y_1 = \frac{1}{\Omega_1}\{-(1+\Delta_1)X_1 + Y_1\}$$
$$x_2 = X_2, \quad y_2 = \frac{1}{\Omega_2}\{-(1+\Delta_2)X_2 + Y_2\},$$
$$\tau = \Omega_1\tau', \quad \text{“}\cdot\text{”} = \frac{d}{d\tau}. \tag{6}$$

Equation (4) can be transformed into the following Jordan form [22]:

$$\begin{bmatrix} \dot{x_1} \\ \dot{y_1} \end{bmatrix} = \begin{bmatrix} \delta_1 & 1 \\ -1 & \delta_1 \end{bmatrix}\left[\begin{bmatrix} x_1 \\ y_1 \end{bmatrix} - \eta\begin{bmatrix} p_1 \\ m_1p_1 \end{bmatrix}h(x_1+x_2)\right],$$
$$\begin{bmatrix} \dot{x_2} \\ \dot{y_2} \end{bmatrix} = \begin{bmatrix} \delta_2 & \omega_2 \\ -\omega_2 & \delta_2 \end{bmatrix}\left[\begin{bmatrix} x_2 \\ y_2 \end{bmatrix} - \eta\begin{bmatrix} p_2 \\ m_2p_2 \end{bmatrix}h(x_1+x_2)\right], \tag{7}$$

where seven parameters $(\delta_1, \delta_2, \omega_2, p_1, m_1, p_2, m_2)$ are given by

$$\delta_1 = \Delta_1/\Omega_1, \quad \delta_2 = \Delta_2/\Omega_1, \quad (\omega_1 = 1), \quad \omega_2 = \Omega_2/\Omega_1,$$

$$m_1 \equiv \frac{1}{\Omega_1}\{1/\beta_1 - (1+\Delta_1)\}, \quad m_2 \equiv \frac{1}{\Omega_2}\{1/\beta_2 - (1+\Delta_2)\}.$$

Note again that the original parameters are (α_1, β_1, α_2, β_2, η). The equilibrium point moves along the line $\Gamma = \{(\mathbf{x}, h) \mid y_1 = m_1x_1, y_2 = m_2x_2\}$ as η varies. Hereafter, we abbreviate (7) as the following:

$$\dot{\mathbf{x}} = \mathbf{A}(\mathbf{x} - \eta\mathbf{p}h(x_1+x_2)), \tag{8}$$

where

$$\mathbf{x} \equiv (x_1, y_1, x_2, y_2)^T, \quad \mathbf{p} \equiv (p_1, m_1p_1, p_2, m_2p_2)^T,$$

$$\mathbf{A} \equiv \begin{bmatrix} \delta_1 & 1 & 0 & 0 \\ -1 & \delta_1 & 0 & 0 \\ 0 & 0 & \delta_2 & \omega_2 \\ 0 & 0 & -\omega_2 & \delta_2 \end{bmatrix}$$

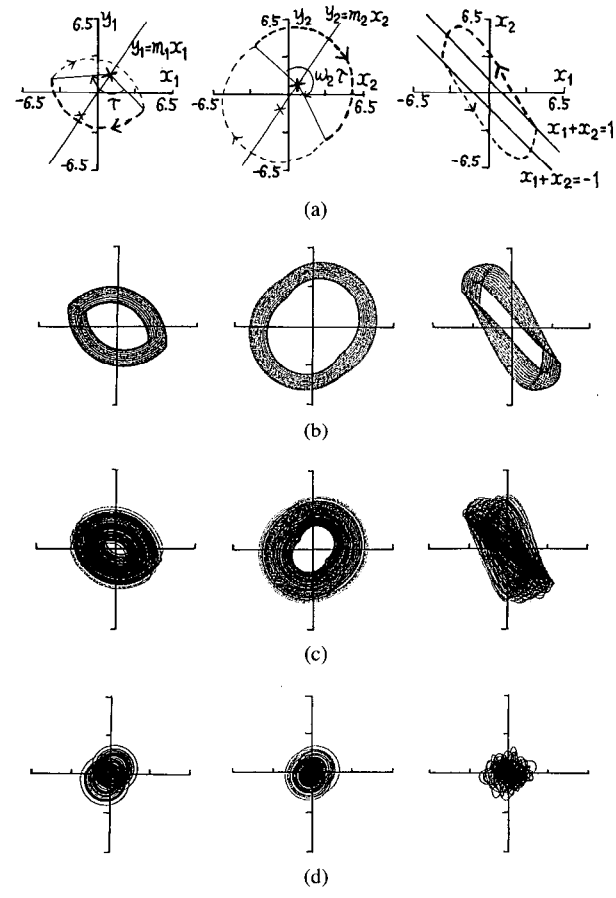

Fig. 3. Change of attractor from Jordan form as η decreases (α_1, β_1, α_2, β_2) = (7.5, 0.16, 15, 0.097) Jordan form parameters: (δ_1, δ_2, ω_2, p_1, m_1, p_2, m_2) = (0.04, 0.09, 1.47, 0.19, 2.05, 0.11, 2.47). (a) Periodicity for $\eta = 3.8$; (b) torus for $\eta = 3.0$; (c) area expanding chaos ($\mu_2 > 0$) for $\eta = 2.0$; (d) volume expanding chaos ($\mu_3 > 0$) for $\eta = 1.3$. This corresponds to Fig. 2.

Solution for $h = 1$ is given by the following and the other is symmetric to it:

$$\mathbf{x}(\tau) - \eta\mathbf{p} = e^{A\tau}(\mathbf{x}(0) - \eta\mathbf{p}), \tag{9}$$

where

$$e^{A\tau} = \begin{bmatrix} e^{A_1\tau} & \mathbf{O} \\ \mathbf{O} & e^{A_2\tau} \end{bmatrix}, \quad e^{A_k\tau} = e^{\delta_k\tau}\begin{bmatrix} \cos\omega_k\tau & \sin\omega_k\tau \\ -\sin\omega_k\tau & \cos\omega_k\tau \end{bmatrix} \quad (k = 1, 2).$$

Fig. 3 shows change of attractor from the Jordan form as η decreases corresponding to Fig. 2. The attractors in Fig. 3 are equivalent to the ones in Fig. 2 through the transformations in (3) and (6). Here, Fig. 3(a) shows a periodic attractor. Bold dot arc is on the upper branch $h = 1$, and fine dot one is on the lower branch -1. Its moving angles are τ in (x_1, y_1) plane and $\omega_2\tau$ in (x_2, y_2) plane, respectively, where $\omega_1 = 1$ and $\omega_2 = 1.47$ in this example.

An interaction between two angular frequencies ω_1 and ω_2 affects the switching dynamics. In this case ω_2 is higher than ω_1, trajectory on (x_2, y_2) plane rotates faster than that in (x_1, y_1) plane. When the trajectory forms the lower arc on (x_1, y_1) plane, it forms the upper arc on (x_2, y_2) plane. Such proportion is destroyed as a parameter varies. Thus x_1 has inverse correlation to x_2. For a simplicity on the experiment,

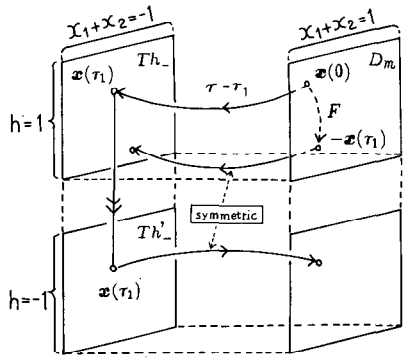

Fig. 4. Abstract figure of 3-D return map by projection of 4-D halfspaces connected to each other by hysteresis switching.

we select η as a control parameter that can be adjusted by only r_b. As η decreases, the equilibrium point approaches to the origin. Then the attractor can not keep the proportion between both arcs and changes to torus Fig. 3(b), and then to chaotic ones Fig. 3(c) and (d). From Fig. 3(a) to (c), the attractor has the inverse correlation between x_1 and x_2. But in Fig. 3(d), because some trajectory segments rotate many times around the equilibrium point, it does not have such correlation. In next section, we investigate this change quantitatively.

III. Return Map and its Lyapunov Exponents

In order to derive the return map according to [19], we define some objects (see Fig. 4):

$$\begin{aligned} D_m &= \{(\mathbf{x}, h) \mid x_1 + x_2 = 1,\ h = 1\} \\ \mathrm{Th}_- &= \{(\mathbf{x}, h) \mid x_1 + x_2 = -1,\ h = 1\} \\ \mathrm{Th}'_- &= \{(\mathbf{x}, h) \mid x_1 + x_2 = -1,\ h = -1\} \end{aligned} \tag{10}$$

where D_m, Th_- and Th'_- are domain of the return map, left threshold of h and projection of Th'_-, respectively. Note that Fig. 4 is an abstract figure of 4-D halfspaces connected to each other by hysteresis switching. Let any point in D_m be represented by its y_2, x_2 and y_2 coordinates.

We consider the case where the trajectory starting from $\mathbf{x}(0)$ in D_m hits a point $\mathbf{x}(\tau_1)$ in Th_- and jumps to the same point in Th'_-, where τ_1 is the switching time. Since the vector field is symmetric, the trajectory starting from $\mathbf{x}(\tau_1)$ in Th'_- is symmetric to that starting from $-\mathbf{x}(\tau_1)$ in D_m. Then, we can define the following 3-D return map:

$$F : D_m \mapsto D_m,$$

$$(y_1(0), x_2(0), y_2(0)) \mapsto -(y_1(\tau_1), x_2(\tau_1), y_2(\tau_1)). \tag{11}$$

Image of F is given by:

$$(y_1(\tau_1), x_2(\tau_1), y_2(\tau_1))^T = \mathbf{S}(e^{A\tau}(\mathbf{x}(0) - \eta\mathbf{p}) + \eta\mathbf{p}), \tag{12}$$

where

$$\mathbf{S} \equiv \begin{bmatrix} 0 & 1 & 0 & 0 \\ 0 & 0 & 1 & 0 \\ 0 & 0 & 0 & 1 \end{bmatrix}.$$

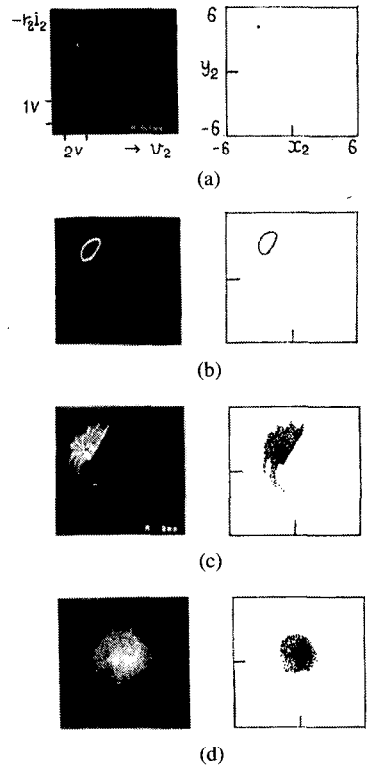

Fig. 5. Projections of attractors from the return map ($C \simeq 10$ nF, $R \simeq 15$ kΩ, $L_1 \simeq 300$ mH, $L_2 \simeq 150$ mH, $r_1 \simeq 2.5$ kΩ, $r_2 \simeq 1.5$ kΩ). Normalized parameters: $(\alpha_1, \beta_1, \alpha_2, \beta_2) = (7.5, 0.16, 15, 0.097)$. (a) Periodicity for $\eta = 3.8$; (b) torus for $\eta = 3.0$; (c) area expanding chaos ($\mu_2 > 0$) for $\eta = 2.0$; (d) volume expanding chaos ($\mu_3 > 0$) for $\eta = 1.3$. • This corresponds to Figs. 2 and 3.

Here, the switching time τ_1 can be given by the following implicit equation:

$$\mathbf{w}(e^{A\tau}(\mathbf{x}(0) - \eta\mathbf{p}) + \eta\mathbf{p}) = -1, \tag{13}$$

where

$$\mathbf{w} \equiv (1, 0, 1, 0).$$

In actual calculations, it can be solved by using the Newton-Raphson method. We obtain the image of the map by substituting this τ_1 into (12).

Fig. 5 shows the attractors from the return map given by both laboratory and numerical experiments. It corresponds to the attractors in Figs. 2 and 3. They are projections to $(v_1, -r_1 i_1)$ and (x_2, y_2) spaces, respectively. The laboratory measurements can be realized by the following procedure:

1) A comparator with threshold voltage zero bipolarizes ($-H = E$ corresponds to $h = 1$).
2) The comparator output is transformed to trigger pulse by a differentiator.
3) The differentiator output is applied to the luminous modulation terminal in the oscilloscope.

In Fig. 5(b), the attractor forms a closed curve. Therefore, it is torus. The chaotic attractor in Fig. 5(d) is more complicated than that in Fig. 5(c).

In order to calculate Lyapunov exponents for attractor from the return map, we introduce following two theorems.

Theorem 1: Let $\mathbf{DF}$ be the Jacobian matrix of the return map. It can be calculated by

$$\mathbf{DF} = \mathbf{S}\left(\mathbf{I} - \frac{\mathbf{A}(\mathbf{x}(\tau_1) - \eta\mathbf{p})\mathbf{w}}{\mathbf{w}\mathbf{A}(\mathbf{x}(\tau_1) - \eta\mathbf{p})}\right)e^{A\tau_1}\mathbf{T}, \tag{14}$$

where $\mathbf{I}$ is identify, and

$$\mathbf{T} = \begin{bmatrix} 0 & -1 & 0 \\ 1 & 0 & 0 \\ 0 & 1 & 0 \\ 0 & 0 & 1 \end{bmatrix}.$$

Theorem 2: The Jacobian $|\mathbf{DF}|$ can be calculated by following formula:

$$|\mathbf{DF}| = |e^{A\tau_1}|\frac{\mathbf{w}\mathbf{A}(\mathbf{x}(0) - \eta\mathbf{p})}{\mathbf{w}\mathbf{A}(\mathbf{x}(\tau_1) - \eta\mathbf{p})}. \tag{15}$$

The proof of these theorems are shown in Appendix. These formulas are calculated by using the image $\mathbf{x}(\tau_1)$, the initial point $\mathbf{x}(0)$ and the switching time τ_1. They can be developed easily to general dimensional cases.

Using these formulas, we can evaluate Lyapunov exponents [23], [24] for attractor from the return map. Hereafter, we classify chaotic phenomena by the Lyapunov exponents from the return map. The map is 3-D and let μ_1, μ_2 and μ_3 be the largest one dimensional, the largest 2-D and 3-D Lyapunov exponent, respectively. They can be calculated by

$$\begin{aligned} \mu_3 &= \frac{1}{N}\sum_{j=1}^{N}\ln|\mathbf{DF}_j| \\ \mu_2 &= \frac{1}{N}\sum_{j=1}^{N}\ln|\mathbf{DF}_j e_1^j \times \mathbf{DF}_j e_2^j| \\ \mu_1 &= \frac{1}{N}\sum_{j=1}^{N}\ln|\mathbf{DF}_j e_1^j| \end{aligned} \tag{16}$$

where e_1^j and e_2^j are orthonormal bases and they can be calculated by using the procedure in [23]. Note that (15) is useful to calculate μ_3.

If μ_1 is positive then the return map expands the line, if μ_2 is positive then it expands the area, and if μ_3 is positive then it expands the volume, respectively. Then, we can classify the chaos as the following:

1) If $\mu_1 > 0 > \mu_2$, then the attractor is line expanding chaos.
2) If $\mu_2 > 0 > \mu_3$, then the attractor is area expanding chaos.
3) If $\mu_3 > 0$, then the attractor is volume expanding chaos.

Here, the area expanding chaos implies that the map expands no volume but area. Also, the line expanding chaos implies that the map expands neither volume nor area but line.

IV. Route to Chaos in the Hysteresis System

For a simplicity, we select η as the control parameter and the other parameters (α_1, β_1, α_2, β_2) are fixed. The equilibrium point is on the line $\Gamma = \{(\mathbf{x}, h) \mid y_1 = m_1x_1, y_2 = m_2x_2\}$ and it approaches to the origin as η decreases.

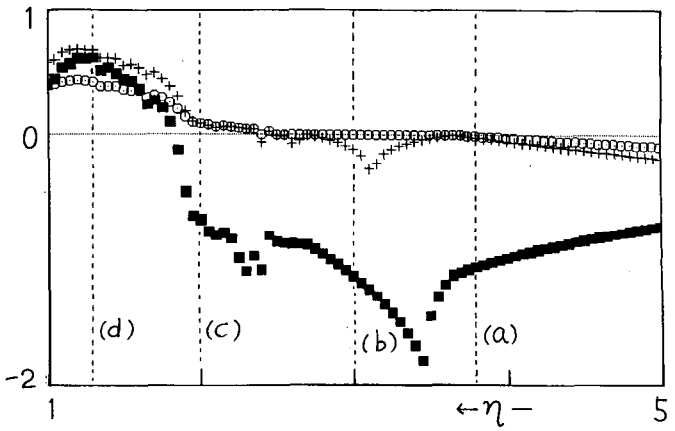

Fig. 6. Lyapunov exponents (α_1, β_1, α_2, β_2) = (7.5, 0.16, 15, 0.097). ○ = Largest 1-D exponents μ_1, + = Largest 2-D exponents μ_2, □ = 3-D exponent μ_3. Attractors (a) to (d) in Fig. 5 are observed at (a) to (d) in this figure.

Fig. 6 shows the Lyapunov exponents for the return map attractors. In this calculation, we have confirmed that the exponents reasonably converged in about 10 000 iterations. So we calculate Lyapunov exponents by using 10 000 iterations after 5000 steps. Here, the attractors (a) to (d) in Fig. 5 are observed at Fig. 6(a) to (d), respectively. At Fig. 6(b), the attractor is torus hence μ_1 is zero. At Fig. 6(c), μ_2 is positive and the attractor is area expanding chaos. At Fig. 6(d), μ_3 is positive and the attractor is volume expanding chaos.

Then, we show a rough scenario for these transitions as η decreases:

1) (a) → (b): The periodic attractor changes to torus via Hopf bifurcation. we have confirmed that e^{μ_1} crosses the unit circle at Hopf bifurcation set.
2) (b) → (c): The transition from torus to area expanding chaos is due to the doubling of torus [25], [26]. We have confirmed torus rolled four times in laboratory experiments (see Fig. 7). If we perform more precise experiment, the torus rolled more times seems to be observed. Fig. 8 shows the Lyapunov exponents in this transition. Here, Torus rolled two times and four times are observed in Fig. 8(e) and (f), respectively.
   In the flow in a 3-D phase space (e.g., Rössler's spiral), period doubling causes transition from periodicity to chaos. Then 1-D Lyapunov exponent changes from negative to positive. Therefore, if torus doubling to chaos takes place in a 3-D return map, μ_2 changes from negative to positive. The line expanding chaos can not be observed in the transition. We can see the above in Fig. 8.
3) (c) → (d): Area expanding chaos changes to volume expanding chaos. As shown in Figs. 2 and 3, the volume expanding chaos has different topology from the area expanding chaos. In the volume expanding chaos, the trajectory arcs can be classified into two categories as shown in Fig. 9(I). Arcs (a) and (b) represent the first and second categories, respectively. (a) Touches Th_-, and (b) does not touch that. Arc (a) has longer switching

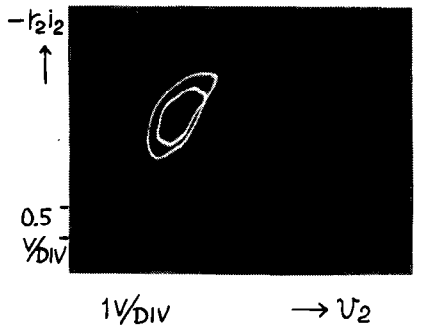

(a)

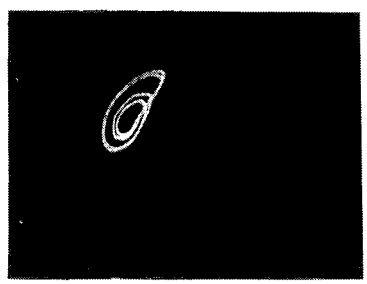

(b)

Fig. 7. Attractors from the return map in torus doubling ($C \simeq 10$ nF, $R \simeq 15$ kΩ, $L_1 \simeq 300$ mH, $L_2 \simeq 150$ mH, $r_1 \simeq 2.5$ kΩ, $r_2 \simeq 1.5$ kΩ). Normalized parameters: $(\alpha_1, \beta_1, \alpha_2, \beta_2) = (7.5, 0.16, 15, 0.097)$ (a) Torus rolled two times for $\eta \simeq 2.6$; (b) torus rolled four times for $\eta \simeq 2.52$.

interval of h than (b). The longer switching interval corresponds to the longer arc. This figure includes the region $\Psi \equiv \{\mathbf{x} \mid x_1+x_2 = 1,\ \dot{x}_1+\dot{x}_2 = 0\}$ on which the trajectory touches Th_-. Note that $0 < \delta_1, \delta_2 \ll 1$ (in this figure, $\delta_1 = 0.04$ and $\delta_2 = 0.09$). If the attractor includes Ψ, such longer trajectory is born. We have confirmed that the area expanding chaos does not includes the longer trajectory segment. Fig. 9(II) shows an example of projection of the return map attractor for volume expanding chaos and it includes Ψ. Fig. 9(III) shows that for area expanding chaos and it excludes Ψ.

Then we have calculated a rough two parameters bifurcation diagram as shown in Fig. 10. Here, we note that α_2 is proportional to L_2 and it controls the second resonance frequency. The bifurcation shown in Fig. 5 is observed along the dotted line. This figure suggests that the torus doubling route to chaos is not singular.

V. Conclusion

We have considered a 4-D plus hysteresis chaos generator. The circuit dynamics are described by two symmetric 4-D linear equations connected to each other by hysteresis switchings. We have transformed the circuit equation into Jordan form and have derived theoretical formulas of its 3-D return map, its Jacobian matrix and its Jacobian. These formulas can be developed easily to general dimensional cases. They are used to evaluate Lyapunov exponents. Then we have discovered torus doubling route to area expanding chaos and volume expanding chaos. Some of the return map attractor have been confirmed by laboratory experiments. We have also

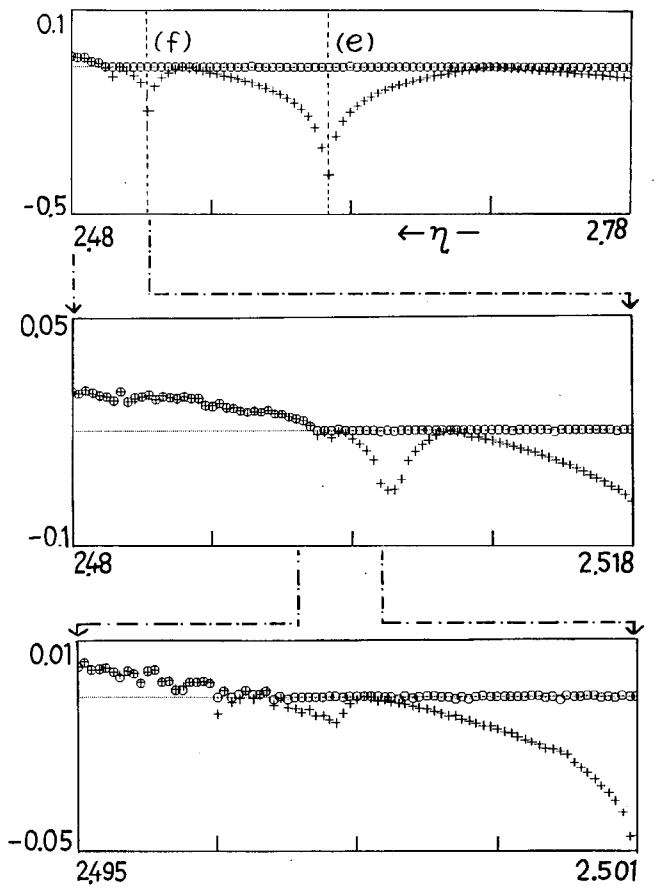

Fig. 8. Lyapunov exponents in torus doubling $(\alpha_1, \beta_1, \alpha_2, \beta_2) = (7.5, 0.16, 15, 0.097)$. ○ = Largest 1-D exponents μ_1, + = Largest 2-D exponents μ_2, • Attractors (a) and (b) in Fig. 7 are observed at (e) and (f) in this figure.

calculated a rough two parameters bifurcation diagram. Then we enumerate following future problems:

1) In order to analyze the bifurcations in more detail, interaction between two frequencies ω_1 and ω_2 should be investigated. If the two frequencies match each other, the attractor is to be periodic. As parameter varies, this matching is destroyed and the complicated phenomena are caused.
2) Much more complicated but interesting phenomena may occur in higher odd dimensional systems which includes many resonance frequencies $(\omega_1, \omega_2, \ldots, \omega_N)$. Our systematic analysis procedure may enable us to approach to higher dimensional systems.
3) We should try to apply the hysteresis system for some engineering applications, e.g. spread spectrum communications and controlling chaos. Especially, a basic application for controlling chaos will be published elsewhere.

Appendix I
The Derivation of Jacobian Matrix DF

First, we introduce the following:

$$\mathbf{U} \equiv \mathbf{x}(0), \quad \mathbf{V} \equiv \mathbf{x}(\tau_1) \tag{17}$$

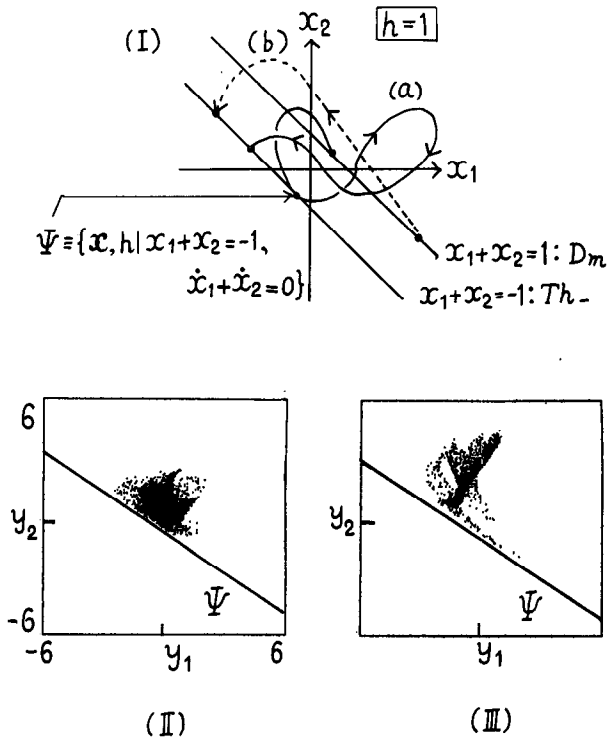

Fig. 9. Characterizing volume expanding chaos. (I) Two kinds of trajectories, trajectory (a) touches Th_- and (b) does not touch it. (II) The projection of the return map attractor in volume expanding chaos for $\eta = 1.3$; (III) that in area expanding chaos for $\eta = 2.0$.

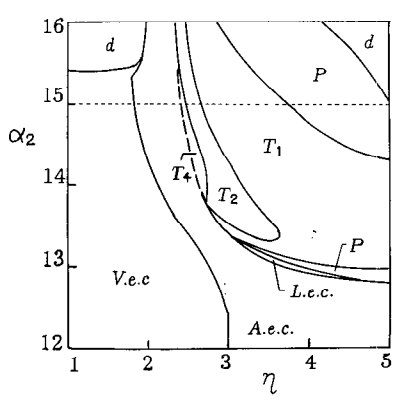

Fig. 10. Two parameters bifurcation diagram $(\alpha_1, \beta_1, \beta_2) = (7.5, 0.16, 0.097)$. P: periodic attractor, Tn: torus rolled n times, L.e.c: line expanding chaos, A.e.c: area expanding chaos, V.e.c: volume expanding chaos, d: divergence. The broken curve is torus doubling bifurcation set. The bifurcation in Fig. 6 is observed along the dotted line.

Using the above, we recast (11) into the following:

$$F : (U_2, U_3, U_4) \to -(V_2, V_3, V_4) \tag{18}$$

$$\text{ab. } F : \mathbf{u} \to -\mathbf{v} \text{ where, } \mathbf{u} = \mathbf{SU}, \quad \mathbf{v} = \mathbf{SV}$$

Next, we define the following functions:

$$\begin{aligned} &\mathbf{f}(\mathbf{u}, \tau_1(\mathbf{u})) \equiv \mathbf{S}(e^{A\tau}(\mathbf{U} - \eta\mathbf{p}) + \eta\mathbf{p}), \mathbf{w}(\mathbf{U} - \eta\mathbf{p}) = 1, \\ &g(\mathbf{u}, \tau_1(\mathbf{u})) \equiv \mathbf{w}(e^{A\tau}(\mathbf{U} - \eta\mathbf{p}) + \eta\mathbf{p}) + 1 = 0. \end{aligned} \tag{19}$$

Differentiating both sides of $\mathbf{f}$, we have:

$$\begin{aligned} -\mathbf{DF} &= \frac{\partial(V_2, V_3, V_4)}{\partial(U_2, U_3, U_4)} = \frac{\partial f}{\partial \mathbf{u}} \\ &= \mathbf{S}e^{A\tau_1}\frac{\partial \mathbf{U}}{\partial \mathbf{u}} + \mathbf{SA}e^{A\tau_1}(\mathbf{U} - \eta\mathbf{p})\frac{\partial \tau_1}{\partial \mathbf{u}} \end{aligned} \tag{20}$$

Noting that $U_1 = -U_3 + \eta(p_1 + p_2) + 1$:

$$\mathbf{S}e^{A\tau_1}\frac{\partial \mathbf{U}}{\partial \mathbf{u}} = \mathbf{S}e^{A\tau_1}\mathbf{T} \tag{21}$$

Applying theorem on implicit function for $g = 0$, we obtain:

$$\frac{\partial \tau_1}{\partial \mathbf{u}} = -\frac{\partial g}{\partial \mathbf{u}} \Big/ \frac{\partial g}{\partial \tau_1} = -\frac{\mathbf{w}e^{A\tau_1}\mathbf{T}}{\mathbf{wA}e^{A\tau_1}(\mathbf{U} - \eta\mathbf{p})} \tag{22}$$

where note that the denominator of the above is the velocity of $\mathbf{w}(\mathbf{V} - \eta\mathbf{p})$ and it is negative because $\mathbf{wx}(= x_1 + x_2)$ hits -1 from the right at $\tau = \tau_1$. Substituting (21) and (22) into (20), we obtain (14).

Appendix II
The Derivation of Jacobian $|\mathbf{DF}|$

Noting (12), first we define:

$$\mathbf{G}(\tau_1(\mathbf{u}), \mathbf{u}, \mathbf{v}(\mathbf{u})) \equiv e^{A\tau}(\mathbf{U} - \eta\mathbf{p}) - (\mathbf{V} - \eta\mathbf{p}) \tag{23}$$

Differentiating $\mathbf{G} = 0$ by $(\tau_1, \mathbf{u})$, we obtain:

$$\frac{\partial \mathbf{G}}{\partial(\tau_1, \mathbf{u})} + \frac{\partial \mathbf{G}}{\partial(\tau_1, \mathbf{v})}\frac{\partial(\tau_1, \mathbf{v})}{\partial(\tau_1, \mathbf{u})} = 0 \tag{24}$$

ab. $\mathbf{K} + \mathbf{LX} = 0$, $(|\mathbf{L}||\mathbf{X}| = |-\mathbf{K}|)$, where

$$\mathbf{K} = \left[\frac{\partial \mathbf{G}}{\partial \tau_1}\frac{\partial \mathbf{G}}{\partial \mathbf{u}}\right] = e^{A\tau_1}\left[\mathbf{A}(\mathbf{U} - \eta\mathbf{p}) \quad \begin{matrix} 0 & -1 & 0 \\ 1 & 0 & 0 \\ 0 & 1 & 0 \\ 0 & 0 & 1 \end{matrix}\right] \tag{25}$$

$$\mathbf{L} = \left[\frac{\partial \mathbf{G}}{\partial \tau_1}\frac{\partial \mathbf{G}}{\partial \mathbf{v}}\right] = \left[\mathbf{A}(\mathbf{V} - \eta\mathbf{p}) \quad \begin{matrix} 0 & 1 & 0 \\ -1 & 0 & 0 \\ 0 & -1 & 0 \\ 0 & 0 & -1 \end{matrix}\right] \tag{26}$$

$$\mathbf{X} = \begin{bmatrix} \partial\tau_1/\partial\tau_1 & \partial\tau_1/\partial\mathbf{u} \\ \partial\mathbf{v}/\partial\tau_1 & \partial\mathbf{v}/\partial\mathbf{u} \end{bmatrix} = \begin{bmatrix} 1 & \partial\tau_1/\partial\mathbf{u} \\ \mathbf{O} & -\mathbf{DF} \end{bmatrix} \tag{27}$$

Using Cramer's formula, we obtain:

$$|-\mathbf{K}| = |e^{A\tau_1}|\mathbf{wA}(\mathbf{U} - \eta\mathbf{p}) \tag{28}$$

$$|\mathbf{L}| = -\mathbf{wA}(\mathbf{V} - \eta\mathbf{p}) \tag{29}$$

Substituting these into $|-\mathbf{K}|/|\mathbf{L}| = |\mathbf{X}| = -|\mathbf{DF}|$, we obtain (15).

REFERENCES

[1] A. S. Pikovski and M. I. Rabinovich, "Stochastic oscillation in dissipative systems," *Physica D*, vol. 2, pp. 8–24, 1981.

[2] R. W. Newcomb and N. El-Leithy, "Binary h ysteresis chaos generator," in *Proc. IEEE/ISCAS*, 1984, pp. 856–859.

[3] L. O. Chua, C. W. Wu, A. Huang, and G. Q. Zhong, "A universal circuit for studying and generating chaos—part I: Route to chaos," *IEEE Trans Circuits Syst.*, vol. 40, no. 10, pp. 732–744, 1993.

[4] T. Matsumoto, L. O. Chua, and R. Tokunaga, "Chaos via torus break down," *IEEE Trans Circuits Syst.*, vol 34, pp. 240–253, 1987.

[5] T. Saito, "On chaos generator described by a piecewise linear constrained equation," *Trans. IEICE*, J71-A, vol. 4, pp. 965–972, 1988.

[6] T. Matsumoto, L. O. Chua, and K. Kobayashi, "Hyperchaos: Laboratory experiment and numerical confirmation," *IEEE Trans. Circuits Syst.*, vol. 33, no. 11, pp. 1143–1147, 1986.

[7] O. E. Rössler, "Continuous chaos—four prototype equations," in *Bifurcation Theory and Applications in Scientific Disciplines, Annals of the New York Academy of Sciences*, vol. 316, pp. 376–392, 1979.

[8] T. Saito, "Reality of chaos in four dimensional hysteretic circuits," *IEEE Trans. Circuits Syst.*, vol. 38, no. 12, pp. 1517–1524, 1991.

[9] N. Kutsuzawa, Y. Nishio, T. Saito, N. Inaba, and S. Mori, "Chaotic phenomena in higher dimensional ladder circuit," *ECCTD*, Sep. 1993.

[10] E. N. Lorenz, "The local structure of a chaotic attractor in four dimensions," *Physica 13D*, pp. 90–104, 1984.

[11] J. L. Hudson, O. E. Rössler and H. C. Killory, "Chaos in a four variables piecewise linear system of differential equations," *IEEE Trans. Circuits Syst.*, vol. 35, no. 7, pp. 902–908, 1988.

[12] K. S. Halle, C. W. Wu, M. Itoh, and L. O. Chua, "Spread spectrum communication through modulation of chaos," *Int. J. Bifurcation and Chaos*, vol. 3, no. 2, pp. 469–477, 1993.

[13] M. J. Ogorzalek, "Taming chaos: Part I—synchronization," *IEEE Trans. Circuits Syst.*, vol. 40, no. 10, pp. 693–699, 1993.

[14] W. L. Ditto, S. N. Rauseo, and M. L. Spano, "Experimental control of chaos," *Phys. Rev. Lett.*, vol. 65, no. 26, pp. 3211–3214, 1990.

[15] W. L. Ditto and L. M. Pecora, "Mastering chaos," *Sci. Amer.*, Aug. 1993.

[16] M. J. Ogorzalek, "Taming chaos: Part II—control," *IEEE Trans. Circuits Syst.*, vol. 40, no. 10, pp. 700–706, 1993.

[17] S. Nara, P. Davis, and H. Totsuji, "Memory search using complex dynamics in a recurrent neural network model," *Neural Networks*, vol. 6, no. 7, pp. 963–973, 1993.

[18] T. Saito, "A chaos generator based on a quasi-harmonic oscillator," in *Proc. IEEE/ISCAS*, 1984, pp. 107–110.

[19] ——, "An approach toward higher dimensional hysteresis chaos generators," *IEEE Trans. Circuits Syst.*, vol. 37, no. 3, pp. 399–409, 1990.

[20] M. Komuro, R. Tokunaga, T. Matsumoto, L. O. Chua, and A. Hotta, "Global bifurcation analysis of the double scroll circuit," *Int. J. Bifurcation and Chaos*, vol. 1, no. 1, pp. 139–182, 1991.

[21] L. O. Chua, "Chua's circuit: Ten years later," in *Proc. NOLTA Workshops*, Hawaii, pp. 9–24, 1993.

[22] J. Guckenheimer and P. Holmes, *Nonlinear Oscillations, Dynamical Systems, and Bifurcations of Vector Fields*. New York: Springer-Verlag, 1983, p. 9.

[23] I. Shimada and T. Nagashima, "A numerical approach to ergodic problem of dissipative dynamical systems," *Prog. Theor. Phys.*, vol. 61, pp. 1605–1615, 1979.

[24] J. D. Farmer, E. Otto, and J. A. Yorke, "The dimension of chaotic attractors," *Physica 7D*, pp. 153–180, 1983.

[25] K. Kaneko, "Oscillation and doubling of torus," *Prog. Theor. Phys.*, vol. 72, pp. 202–215, 1984.

[26] N. Inaba and S. Mori, "Bifurcations of tori and chaos in a coupled chaos generating circuit," *Trans. IEICE*, vol. J72-A, no. 3, pp. 614–617, 1989.

[27] T. Suzuki and T. Saito, "On fundamental bifurcation from a hysteresis hyperchaos generator," *IEEE Trans. Circuits Syst.*, this issue, pp. 876–884.

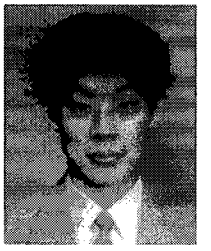

Kunihiko Mitsubori received the B.E. and M.E. degrees in electrical engineering from Hosei University, Tokyo, Japan, in 1992 and 1994, respectively. He is currently working towards the Ph.D. degree in electrical engineering.

His interests are in chaotic circuits and their applications

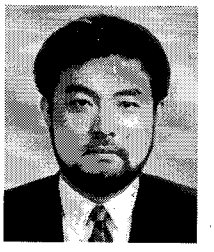

Toshimichi Saito (M'89) received the B.E., M.E., and Ph.D. degrees in electrical engineering from Keio University, Yokohama, Japan, in 1980, 1982 and 1985, respectively.

He is currently an Associate Professor of Electrical Engineering at Hosei University, Tokyo, Japan. His interests are in chaos and artificial neural networks.